Search for radiative transitions in the hypernucleus Λ^{10}B

R. E. Chrien, S. Bart, M. May, P. H. Pile, and R. J. Sutter
Brookhaven National Laboratory, Upton, New York 11973

P. Barnes, B. Bassalleck,[a] R. Eisenstein,[b] G. Franklin, R. Grace,[c] D. Marlow,[d]
R. Rieder, J. Seydoux, J. Szymanski,[e] and W. Wharton[f]
Carnegie-Mellon University, Pittsburgh, Pennsylvania 15213

J. Derderian[g]
Columbia University, New York, New York 10027

Y. Civelekoglu, M. Deutsch, and J. Prater
Massachusetts Institute of Technology, Cambridge, Massachusetts 02139

C. Chu, R. Hackenburg,[h] E. Hungerford, and T. Kishimoto[i]
University of Houston, Houston, Texas 77204

T. Fukuda[j]
University of Osaka, Toyonaka, Osaka 560, Japan

M. Barlett, G. Hoffman, and E. C. Milner[e]
University of Texas, Austin, Texas 78712

R. L. Stearns
Vassar College, Poughkeepsie, New York 12601
(Received 25 August 1989)

A search for radiative transitions between 0.100 and 0.9 MeV from the p-shell hypernucleus $^{10}_{\Lambda}$B was undertaken. Of special interest are the $M1$ spin-flip transitions between members of the doublet formed by coupling an s-shell Λ hyperon to the nuclear core. No such transitions were observed in this energy range attributable to $^{10}_{\Lambda}$B. This negative result provides additional constraints on the parameters of the p-shell Λ-nucleon effective potential. Evidence is presented of the observation of a γ ray which may be attributed to either the hyperfragment $^{8}_{\Lambda}$Li or $^{8}_{\Lambda}$Be. A cross section for the exclusive reaction ^{7}Li$(\pi,\pi')^{7}$Li* (E_x = 478 keV) of 2.2±0.3 mb/sr was also obtained.

I. INTRODUCTION

A. Radiative transitions in hypernuclei

The role of the radiative transitions in hypernuclei may be readily understood in terms of a weak-coupling model in which the Λ is coupled to a nuclear core consisting of $A-1$ nucleons. For low-energy excitations, the Λ will always be in the s shell, since it is unconstrained by the Pauli exclusion principle. For example for p-shell target nuclei, the configuration will be of the form $(1s)^4_N(1p)^{A-5}_N(1s)_\Lambda$. In general the core states will be split by the spin-dependent interactions of the Λ, as shown in Fig. 1. We may distinguish between two types of transitions. The first is the transition connecting the multiplet partners. This γ ray will be a spin-flip $M1$ transition and will be of relatively low energy, corresponding to the smallness of the spin dependent Λ-nucleon terms. The second is a transition which connects multiplet members built on different core states. This transition is close in energy to the core transition, but is perturbed from that value by the presence of the Λ. It is clear that measurement of either type can provide valuable information on the spin dependence.

The first observations of radiative transitions in hypernuclei were made on hyperfragments produced by stopping negative kaons in beryllium and lithium.[1] Coincidences with emergent pions were subsequently used to identify the hypernucleus involved upon fragmentation of the lithium target.[2] Because of the strength of Λ-particle binding, phase space favors the emission of the mass-4 hyperfragments $^{4}_{\Lambda}$He and $^{4}_{\Lambda}$H; these modes can be distinguished by their pionic-decay modes:

$$^{4}_{\Lambda}\mathrm{H}^{*}\rightarrow{}^{4}_{\Lambda}\mathrm{H}+\gamma,\quad {}^{4}_{\Lambda}\mathrm{H}\rightarrow{}^{4}\mathrm{He}+\pi^{-}\quad (E_{\pi^-}=53\ \mathrm{MeV}), \tag{1}$$

$$^{4}_{\Lambda}\mathrm{He}^{*}\rightarrow{}^{4}_{\Lambda}\mathrm{He}+\gamma,\quad {}^{4}_{\Lambda}\mathrm{He}\rightarrow{}^{4}\mathrm{He}+\pi^{0}\quad (E_{\pi^0}=57\ \mathrm{MeV}). \tag{2}$$

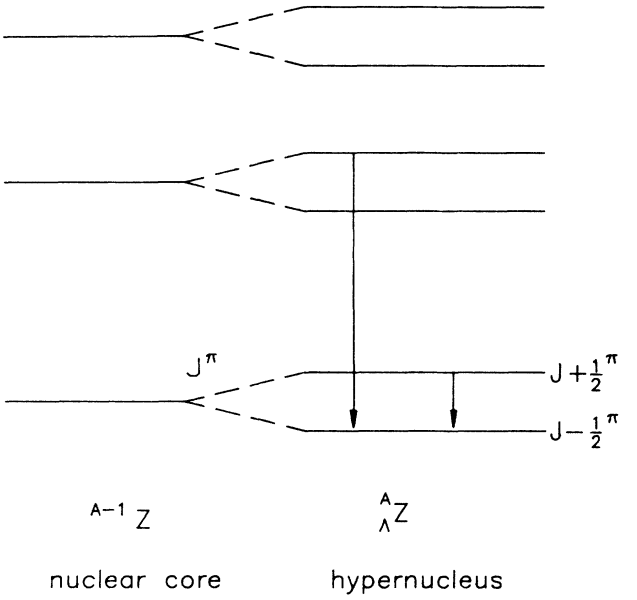

FIG. 1. Two types of hypernuclear radiative transitions; one type, on the right, represents a spin-flip transition connecting multiplet partners, and the other, on the left, represents a core transition modified by the presence of the Λ.

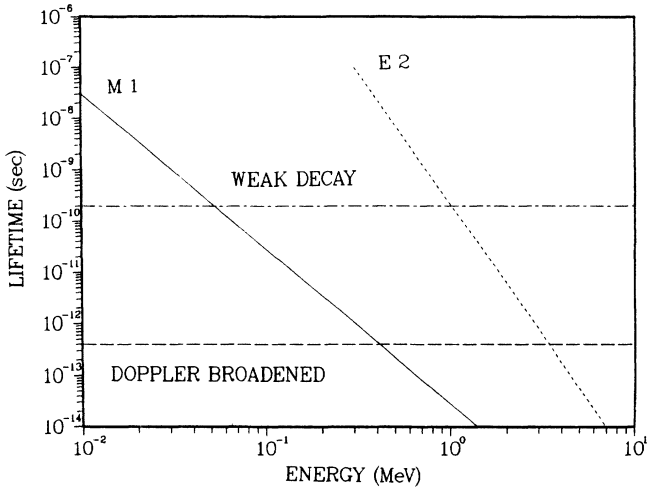

FIG. 2. The range of usefulness for high-resolution hypernuclear spectroscopy. The horizontal lines represent approximate mean times for the weak decay and ionic slowing down times for a typical p-shell hypernucleus. The solid and dotted lines show the approximate $M1$ and $E2$ mean lives as a function of energy, using the conventional single particle expressions. The useful region, for example, is from about 100 to 500 keV for detection of $M1$ spin flip transitions in a p-shell hypernucleus. Below that energy radiation transitions cannot complete against weak decay; above that energy, Doppler broadening will significantly broaden the peak width.

The observations of Bedjidian *et al.*[2] were that the reaction[1] displayed γ rays of energy 1.04 MeV while for Ref. 4 γ rays of 1.15 MeV were observed. These measurements fix the first excited 1^+ states of the mass-4 Λ-hypernuclear systems. Later experiments[3] reported tentatively the existence of a 1.22-MeV γ ray ascribed to ${}^{8}_{\Lambda}$Li.

The first successful in-flight kaon-γ-ray measurements were reported by the Brookhaven collaboration[4] for γ rays in ${}^{7}_{\Lambda}$Li and ${}^{9}_{\Lambda}$Be. In these experiments the strangeness-exchanging (K^-,π^-) reaction was used to access specific states in those hypernuclei. With an array of sodium iodide detectors, hypernuclear transitions from the second excited state of ${}^{7}_{\Lambda}$Li at 2.034 MeV to the ground state, and from the ${}^{9}_{\Lambda}$Be doublet near 3.079 MeV were observed. The former result was interpreted as a core transition in ^{6}Li, i.e., a transition based on the deexcitation of the 2.185 MeV 3^+ ^{6}Li state, slightly perturbed by the presence of an s-shell Λ. The ${}^{9}_{\Lambda}$Be doublet is based on the 3 MeV ^{8}Be 2^+ core state. The failure to resolve the splitting of the 2^+ core state into its $\frac{5}{2}^+$ and $\frac{3}{2}^+$ components was used to place the most severe constraint to date on the size of the two-body ΛN spin-orbit splitting; i.e., $|S_\Lambda| < 0.04$ MeV.[5] The corresponding Λ-nucleus splitting derived from that value is $\epsilon_p < 0.240$ MeV.

It is interesting to note that the mass-4 γ rays were also observed with the in-flight experiment;[4] however, it was not possible to distinguish between the hyperfragments ${}^{4}_{\Lambda}$He and ${}^{4}_{\Lambda}$H.

The γ rays observed in the in-flight experiment on ^{9}Be and ^{7}Li were both interpreted as $E2$ transitions based on a simple model of the s-shell Λ coupled to a nuclear core, i.e., ^{8}Be or ^{6}Li. The observation of the low-energy spin-flip $M1$ connecting the multiplet partners would give a more direct measure of the spin splitting. There is a region of permissible γ-ray energies which allows the effective use of high-resolution germanium diodes. This region, shown in Fig. 2, is bounded on one side by the weak decay lifetime, about 10^{-10} seconds, and on the other by the effects of Doppler broadening. For a narrow range of energies, the lifetime for $M1$ decay is much larger than the slowing down time of hypernuclear recoil. Thus, from Fig. 2, it can be seen that these limits define the useful range for high-resolution detectors between about 100 keV to about 500 keV for the spin-flip $M1$'s. This range, however, encompasses most of the theoretical predictions for doublet spacing described below. Hence, the present experiment was designed to use an array of intrinsic N-type germanium diode detectors.

B. ΛN effective interaction

The theoretical basis for the predictions of γ radiation from p-shell hypernuclei were given in a series of papers by Dalitz, Gal, Soper, Dover, and Millener.[5–9] These authors formulated an intermediate-coupling shell model of p-shell hypernuclei, i.e., those with the configuration $\{(1s)_N^4 (1p)_N^{A-5} (1s)_\Lambda\}$. The formalism was used in an analysis of the separation energies for p-shell hypernuclei in terms of primary ΛN and ΛNN interactions, adjusting the parameters phenomenologically by fitting observed energy-level patterns in these nuclei. The resulting Λ hy-

pernuclear wave functions are used in the calculation of other properties, such as weak decay, production cross sections in (K^-,π^-) reactions, and γ-ray transition strengths. As the experimental database improved, this phenomenological analysis was refined. In the most recent two papers, Dalitz and Gal,[9] and Millener, Gal, Dover, and Dalitz[5] made an extensive set of predictions for the expected energies and strengths of the core and multiplet transitions.

The two-body ΛN interaction is expressed in terms of five radial integrals over harmonic oscillator wave functions, one associated with each term in the interaction

$$V_\Lambda = V_0(r) + V_\sigma(r)\mathbf{S}_N\cdot\mathbf{S}_\Lambda + V_\Lambda(r)\boldsymbol{l}_{N\Lambda}\cdot\mathbf{S}_\Lambda + V_N(r)\boldsymbol{l}_{N\Lambda}\cdot\mathbf{S}_N + V_T(r)S_{12} , \quad (3)$$

where

$$S_{12} = 3(\boldsymbol{\sigma}_N\cdot r)(\boldsymbol{\sigma}_\Lambda\cdot r) - \boldsymbol{\sigma}_N\cdot\boldsymbol{\sigma}_\Lambda . \quad (4)$$

These radial integrals, designated as V, Δ, S_Λ, S_N, and T, respectively, are assumed identical across the p shell, and are termed the spin-averaged-central, the spin-spin, the Λ-spin-orbit, the induced-spin-orbit, and the tensor interactions, respectively. They appear, along with the three-body interaction, in the expressions for the binding energies of the excited states for each hypernuclear species, with coefficients which represent the sum of the two-body Λ-N interaction over the p-shell nucleons involved. Dalitz and Gal[9] concluded the most reasonable fit obtained across the p shell resulted in the parameters 0.15, 0.57, -0.21, and 0.0 MeV for Δ, S_Λ, S_N, and T respectively, while Millener *et al.*[5] used the values 0.50, -0.04, -0.08, and 0.04, for those values. As is apparent from a comparison of these data sets, there is considerable variation in the prediction of the doublet spacings, and in particular the spacings of Ref. 5 predict much smaller spacings than Ref. 9. Several of the closely spaced levels predicted by Ref. 5 are an ideal match for the usefulness of high-resolution germanium diode spectrometers, as they fall within the window described by Fig. 2.

The calculated cross sections for the population of discrete final states of hypernuclei through the (K^-,π^-) are described in some detail in Ref. 8 and also in the comprehensive paper on the nuclear structure of p-shell hypernuclei by Auerbach *et al.*[10] The specific cross sections required here are dealt with in a later section. Expression for transition rates (or lifetimes) are also given in Ref. 8.

II. DESCRIPTION OF EXPERIMENT

A. General description

Gamma rays following the formation of hypernuclei by the strangeness-exchanging (K^-,π^-) reaction were detected using the low-energy separated kaon beam (LESB-1) at the Brookhaven Alternating Gradient Synchrotron. The target was 12.3 g/cm^2 of boron powder (enriched to 93% of ^{10}B), of nominal size $(z,x,y)=(12\times10\times2)$ cm, and encased in a 0.154 cm aluminum sheet. The target was placed at a vertical focus of the beam line tuned to 800 MeV/c negative kaons. The reaction pions were detected with a *QQDQQ* spectrometer system on a rotatable platform; the device is known colloquially as "Moby Dick." The target was subjected to a total irradiation of 2×10^{10} kaons, in the form of beam spills nominally 1.2 s long, occurring every 2.5 s; a typical beam spill contained 5×10^4 kaons in a background of 5×10^5 pions. Data were recorded from an array of six Ge detectors placed around (three above and three below) the sample. The data were preprocessed in a PDP-11 driven *CAMAC* data acquisition system. A fraction of the data—typically 10%, but dependent on count rate—was processed for on-line monitoring; all the data were recorded on magnetic tape and were subsequently replayed for analysis.

Two other auxiliary experiments were performed in aid of the main effort. The reaction ^{7}Li$(\pi,\pi')^7$Li*(478 keV) was studied to assess the performance of the γ-ray detectors in a situation with similar background, but using a known, strong γ-ray transition; a second reaction ^{10}B$(K^-,\pi^-)^{10}_\Lambda$B was performed using a "thin" sample (3.9 g/cm^2) of boron to establish experimentally the reaction cross section for production of the bound states of $^{10}_\Lambda$B. These tests were important in establishing the sensitivity of the experiment.

B. Beam line and spectrometer

The parameters of the Moby Dick spectrometer and LESB-1 beam line relevant to the present experiment are shown in Table I, and the diagram showing the elements and placement of the detectors is displayed in Fig. 3.

The kaon beam incident on the target contains a large contaminant of pions, as indicated in Table I. These pions are rejected efficiently by a Cerenkov veto and timing scintillators. Pions from kaon decay downstream of the target are also rejected by timing, except for a region near the target, where time discrimination is inadequate. As subsequent discussion demonstrates, those decay pions constitute the largest background component in this experiment.

TABLE I. The parameters of the LESB1 beam line and Moby Dick spectrometer (post-1982 version).

p max	1.1 GeV/c beam 1.1 spectrometer
$\Delta p/p$ beam line	±2% (FWHM)
Beam length (meters)	15.2
Separation ratio	10 (π^-/K^-)
(800 MeV/c)	3.5 (π^+/K^+)
Rates/10^{12} protons @ 28 GeV;	45×10^3 (K^-)
6 cm Pt production target	@ 800 MeV/c
Rates (typical) @ 800 MeV/c	135×10^3 (K^-)
Spectrometer resolution	0.2%
$\Delta p/p$ spectrometer	13% (FWHM)
Momentum bite	
Spectrometer rotation	$-5°$ to 45°
$\Delta\Omega$	18 msr

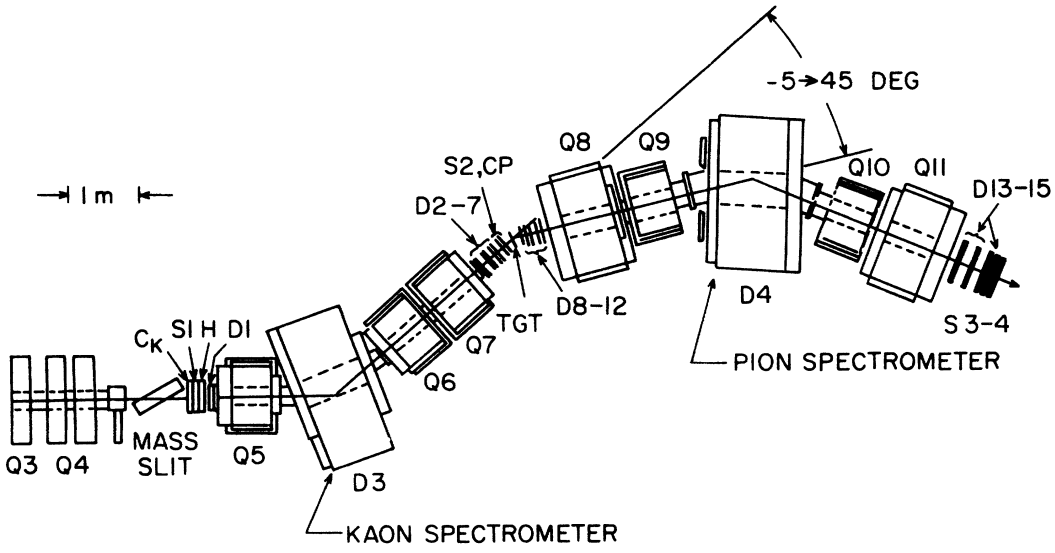

FIG. 3. Diagram of the beam line and Moby Dick spectrometer. Only that portion of the beam line downstream from the mass slit is shown. See text for the meaning of the symbols.

The mass slit hodoscope H and first chamber D1, and chambers D2–D7 define kaon tracking, while D8–D12 and D13–D15 define pion tracking. H consists of 20 9-mm plastic scintillator elements which give horizontal position (bend-plane coordinate x) and timing information. The elements are in two layers overlapped by $\frac{1}{3}$ of their width. By analyzing coincidences between layers the kaon is localized to a 3-mm segment. Figure 4 shows an expanded diagram of the counters in the target region between kaon and pion spectrometers. A complete technical description of the drift chamber and encoding systems has been previously published.[11]

The Cerenkov detectors use lucite radiators; the detector near the target vetoes pions which are produced by kaon decay upstream of the target and which are not distinguishable from kaons by time of flight. The time-of-flight difference between 800-MeV/c pions and kaons over the 5-meter path lengths in the kaon and pion spectrometers is more than 1.3 ns, and the typical rms time resolution provided by the scintillators is about 300 ps in practice. For the large rear scintillators S_3 and S_4, light propagation time effects were eliminated by time averaging the signals from photo tubes at either side of the scintillator. The S_3-S_4 combination was used to reduce neutral particle sensitivity to negligible proportions.

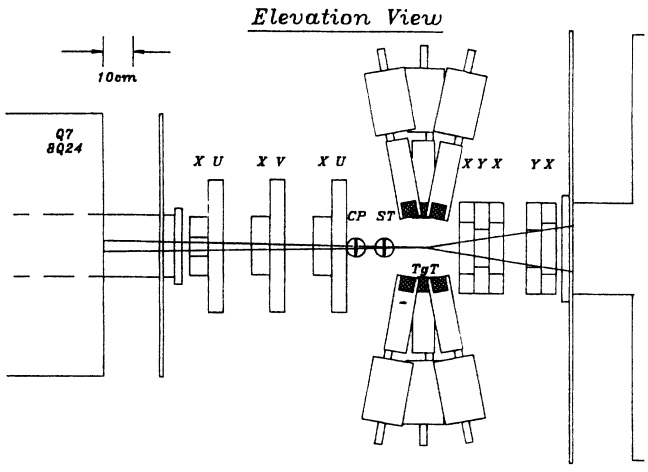

FIG. 4. The configuration of drift chambers and germanium detectors near the target position. C_p and S_T refer to the target Cerenkov detector and trigger scintillator, respectively.

C. Gamma-ray detection apparatus

The theoretical expectations of Refs. 5–9 place certain restrictions on suitable γ-ray detectors. Reasonably high efficiency for energies up to 500 keV must be balanced against good timing characteristics, while the unavoidable large neutron background suggests use of reverse-electrode germanium detectors, which are known to be resistant to radiation damage. The assembly of an array of germanium detectors with their cryostats presents mechanical difficulties. The configuration chosen for this experiment consists of six reverse-electrode coaxial detectors mounted in multiattitude cryostats (Canberra Industries 7935 10.2 cm mini-mac design). The detectors are nominally 50 mm in diameter by 40 mm in depth. These are commercially sold for portable detector applications. The cryostat has a nominal holding time of 8 h with 0.4-liter liquid nitrogen capacity. In the present application, the handles of the cryostat were removed, giving an overall diameter for the housing of 10 cm. A filling system was installed to replenish liquid nitrogen at a 4-h in-

terval. It was convenient to arrange three detectors above and three detectors below the target, as indicated in Fig. 4. A solid angle of 6% of 4π was achievable in this way. The distance from the target to the detector end cap was about 10 cm.

Figure 5 displays a block diagram of the electronics associated with these detectors. Although the detectors were specified to have the typical 2-keV FWHM resolution at 1.33 MeV, in our application the resolution was determined primarily by the ambient electrical noise in the alternating gradient system (AGS) environment and by a mesonic decay halo in the beam which created saturating pulses in the electronics, and consequent baseline perturbations.

The hostile environment led to the adoption of short time constants for the pulse-shaping amplifier, 0.25 μs, followed by the use of a gated integrator with a 2 μs integration time. The beam is surrounded by a halo of decay muons which deposit a large amount of energy in the detector. Typically one observes about 5000 s^{-1} meson-induced events in each diode, each depositing ionization equivalent to a 50-MeV γ ray. The preamplifier must accommodate an average current of 10 nA through the spill. This required a reduction in the input feedback resistor from 2×10^9 to 2×10^8 ohms, resulting in some degradation of detector resolution. Each detector element was wrapped in a three-layer shield consisting of 2.3 mm Pb, 1 mm Cu, and 0.8 mm of Cd. The shield covered the sides of each detector, but the end cap was left unshielded. The intrinsic efficiency for each detector was measured with an antimony-tellurium-europium mixed source (National Bureau of Standards Standard Reference Material 4275). The intrinsic efficiency was typically 80% from 27 keV to about 200 keV, and declined to about 15% at 463 keV. The efficiency was also confirmed *in situ*, after the experiment, by moving the source across the surface of the target and averaging the results to account for detector-target geometry.

A free running, dual-amplitude pulser-injected charge pulses into the preamplifier of each detector randomly across the beam spill macrostructure. The pulses produced peaks in the $(K^-,\pi^-\gamma)$ spectrum which were used to monitor gain stability throughout the duration of the experiment. The pulser proved invaluable in estimating count rate loss due to baseline distortions and dead time due to amplifier recovery after overload. The system resolution as measured with the beam off was 2.8±0.5-keV (FWHM), using the 123-keV γ ray from the NBS source.

With the beam on an appreciable baseline noise contribution is introduced; this was measured at 4-keV FWHM with the pulser, and that noise component dominates the system resolution over the energy range reported in this experiment. Figure 6 shows the annihilation radiation peak as observed in the $(K,\pi\gamma)$ coincidence spectrum. This peak presumably results from π^0 production from K^-- or Λ-decay processes. The fitted resolution function for this peak is 5.6±0.14-keV (FWHM) and contains a $\approx$3-keV Doppler broadening component from the annihilation of positrons.[12] This observation is consistent with the observed pulser resolution and allows us to conclude that the effective γ resolution is a nearly constant 4.5 keV over the range 100–600 keV.

The most important detector characteristic providing discrimination against background is the collection time.

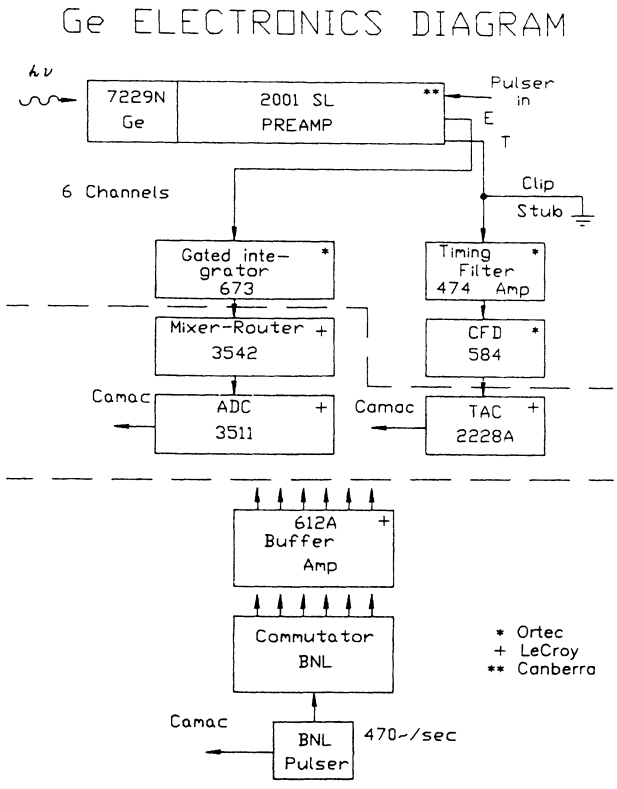

FIG. 5. The electronics block diagram for the γ-ray detection system.

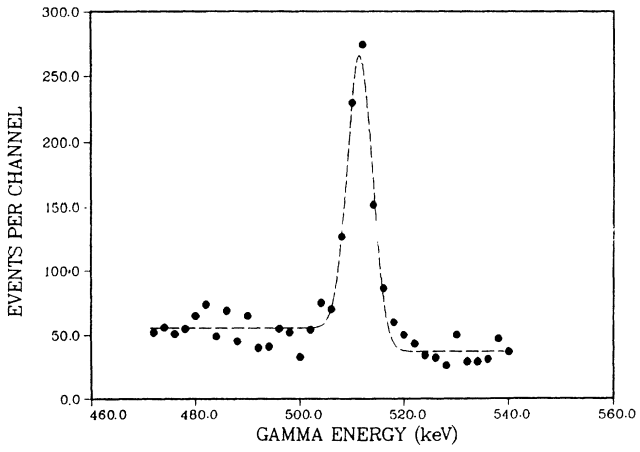

FIG. 6. The observed line shape for the 511-keV annihilation radiation, observed in coincidence with (K^-,π^-) events. The source of this radiation is presumably π^0's originating from either Λ decays, or background K^- decays. The fitted resolution width is 5.6 keV.

This is a strong function of γ-ray energy and influences the detector signal-to-noise ratio dramatically. The detector timing was checked in three ways: (a) out-of-beam with γ-ray sources; (b) in-beam with γ-ray sources; and (c) in-beam with background events. In methods (a) and (b) a ^{133}Ba source was used to trigger a plastic scintillator and the subsequent cascade γ ray was time analyzed. In method (c), the γ-ray continuum, consisting of Compton-scattered photons, in coincidence with a (K^-,π^-) trigger, was analyzed. The coincidence component observed was strong, i.e., a large fraction of the γ-ray continuum is time-coincident with the (K^-,π^-) trigger. It was found that method (a) and (b) gave identical results for time distributions. Figure 7 shows a comparison of methods (b) and (c) for the 81-keV and 356-keV regions, comparing background continuum events for these regions with the photopeaks from a ^{133}Ba source. It is immediately evident that (b) and (c) have the same time distributions. Accordingly, we use method (c) to provide time distributions as a function of γ-ray energy. Figure 8 shows a plot of the results of the continuum timing over the range 0–1 MeV, where the plotted quantity is 4σ, where σ is the time-distribution rms width. This quantity was subsequently chosen as the time acceptance gate for the $(K^-,\pi^-\gamma)$ events in the off-line data analysis.

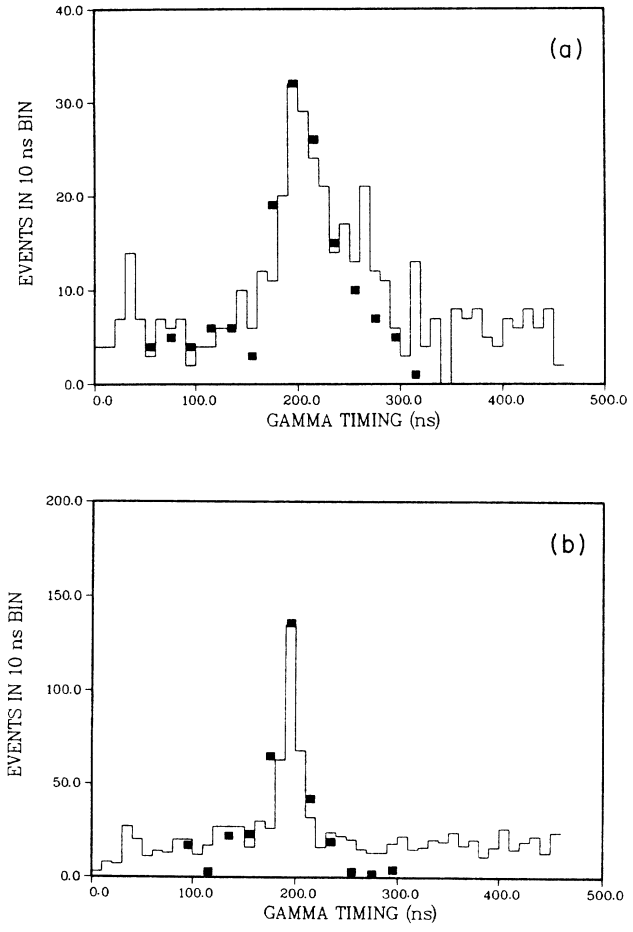

FIG. 7. (a) Two determinations of the time distribution of 81-keV γ rays. The histogram is derived from a selection of continuum events near 81 keV which are coincident with the (K,π) trigger. The points are a result of a measurement with a ^{133}Ba source in the presence of the beam. (b) Same as (a), but for 356-keV γ rays.

III. DATA REDUCTION AND ANALYSIS

The first stage in data analysis is the reduction of drift chamber event data to position and momentum coordinates. Tracks which cannot be reconstructed from the data, as well as some events which do not satisfy rather loosely defined cuts, are rejected at this stage. Next, spatial and timing constraints are applied. A vertex requirement is imposed on the matching of the rear spectrometer track with a straight line segment determined by chambers D2 through D7 in front of the target. Time-of-flight cuts select the incoming and outgoing particle types and a "scattering-angle" cut discards events with reaction angles of less than 10 mrad—so-called straight-through events. These are mainly pions which satisfy the pion spectrometer selection conditions and are counted as kaons because they are in accidental time coincidence with valid kaon beam events.

Subsequent to this selection of physically interesting events, the analysis consists of examining the $M(K^-,\pi^-\gamma)M^*_{HY}$ events which produce γ rays and originate in specific regions of excitation of the resulting hypernucleus.

A major background source which survives to this stage of the analysis is kaon decay. Background events are produced by the decay processes $K^-\rightarrow\pi^0+\pi^-$ and $K^-\rightarrow\mu+\nu$ within the target volume. The former process is particularly troublesome since showers from the π^0 interactions produce time-coincident events in the γ-ray detector array.

The presence of the decay background places a severe constraint on the spectrometer setting. In general the production of bound states of p-shell hypernuclei requires the conversion of a p-shell neutron to an s-shell Λ, or a $\Delta L=1$ transition, which has a cross-section maximum near 15°.[10] This angle lies near the angle where the decay particles from the $K^-\rightarrow\pi^0\pi^-$ and $K^-\rightarrow\mu^-\nu_\mu$ background, whose combined effects are intolerably high, are accepted by the rear spectrometer. Consequently, an effective spectrometer setting of 5°, where the $\Delta L=1$ cross section has about 70% of its maximum value, was selected. Further discrimination against such decay background is achieved, at the expense of some loss of signal, by eliminating events lying along the kinematic trajectory of the decay process in the reaction plane.

Events that are accepted in the (K,π) analysis are sorted into regions of missing mass, corresponding to excitation energies of the recoiling hypernucleus. The γ-ray related descriptors for each region contain energy and timing information. The appropriate time window for each γ-ray energy is selected according to the measurements of Sec. II C. It is important to stress that the cuts of the

K-π analysis are selected independently of the appearance of the γ-ray spectra. Careful studies have shown that fluctuations in the γ-ray spectra can be enhanced by subjective "tuning" of the cuts, and this procedure renders meaningless an objective calculation of the significance level of such a "peak."

The detector amplifiers and analog-to-digital converters (ADC) were calibrated using the ^{133}Ba and NBS standard sources before and after, and at intervals during the run, so that a region from 0–1 MeV was covered in 1000 channels of approximately 1 keV each. The pulser calibration was used in the off-line analysis, as was the ever-present 511-keV annihilation line, to monitor the gain and to make final gain corrections. Simple linear gain and offset corrections were applied to each detector spectrum and they were then summed.

Because of the failure of the gated integrator circuitry to operate properly for very small amplitudes, spurious structures appear at γ-ray energies below 70 keV, and makes this region unsuitable for γ-ray signals. As noted previously, however, in this region γ-ray transitions would not compete against weak decay.

IV. CROSS SECTION DETERMINATION

A. The ^{10}B sample test

The very large target sizes necessary in these γ-ray experiments seriously degrade the momentum resolution of the Moby Dick spectrometer, such that the bound-state region is not well resolved from the continuum region of excitation energy. In order to achieve reliable cross sections for comparison to theory, a thin sample (K,π) spectrum was recorded, so that a well-defined bound-state region could be resolved. The scaling of the "thin-sample" to "thick-sample" runs is then straightforward. The thin-sample run also serves to confirm the effectiveness of data cuts and efficiency calculations.

The cross-section test was carried out with a 3.89 gm/cm^2 thick target of boron enriched to 93% of ^{10}B, run at $\theta=3°$, with $P_{K^-}=800$ MeV/c, and a total irradiation of 5.70×10^8 kaons. The observed (K,π) spectrum for the test is shown in Fig. 9, which indicates that the bound-state region is reasonably resolved from the continuum.

The observed bound-state event rate is related to cross

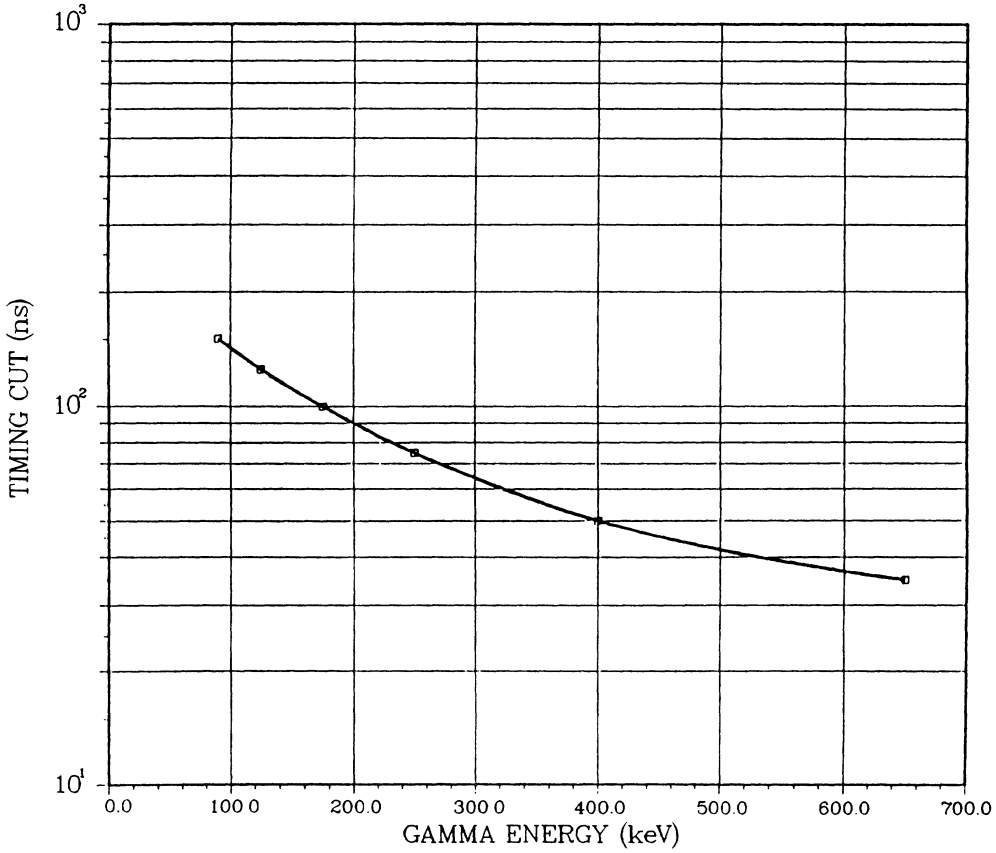

FIG. 8. The time distribution width parameter as a function of γ-ray energy. This parameter was used as the coincidence window in the off-line analysis.

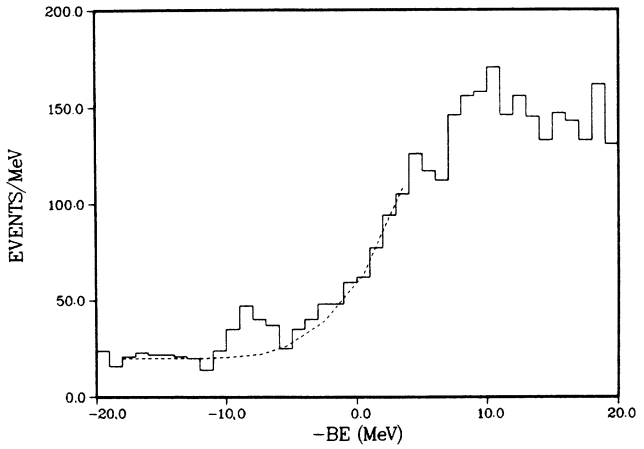

FIG. 9. $^{10}B(K^-,\pi^-)^{10}_{\Lambda}B$ excitation energy spectrum for the thin target. The dashed line indicates the background adopted for the extraction of the bound-state cross section.

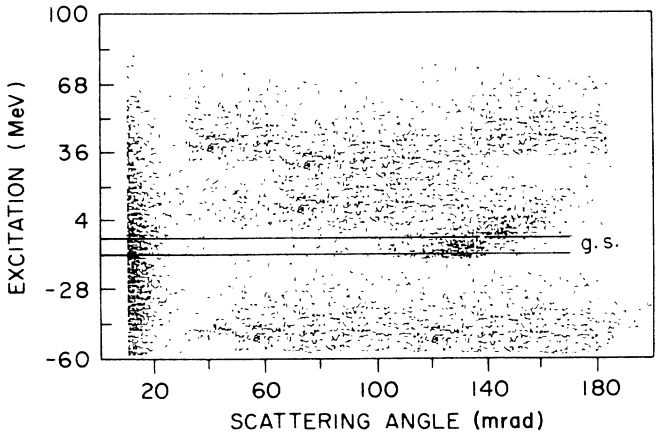

FIG. 10. A density of events plot in the plane defined by the variables excitation energy and scattering angle.

section by

$$N = N_K\,(n\sigma)(\Delta\Omega)\mathrm{eff(SYS)}\,, \tag{5}$$

where N_K is the number of incident kaons, $(n\sigma)$ is the product of areal density of scatterers and cross section, $(\Delta\Omega)$ is the solid angle of the spectrometer (18 msr), and N is the observed counts.

The total system efficiency eff(SYS) is the product of three factors: data acquisition efficiency, spectrometer detector efficiency, and analysis efficiency. The data acquisition efficiency is monitored continuously during the run by recording the total number of triggers which occur during the computer busy gate. The weighted average of the acquisition efficiency in the thin sample run is 0.594. The second factor is the spectrometer efficiency, which is the product of the individual drift chamber efficiencies corrected by redundancy where present. This efficiency may be estimated from the individual detector efficiency, and this was checked also in the $^7\mathrm{Li}(\pi,\pi')^7\mathrm{Li}^*(478)$ test, where the signal γ ray was strong enough to be detectable above background with or without spectrometer tracking. The value of 0.802 ± 0.06 is consistent between these separate estimates.

The third factor results from the application of the three analysis cuts: (1) the z vertex cut, (2) the decay kinematics cut, and (3) the scattering-angle cut to remove spurious events near zero degrees. Those cuts are effective in removing background but they do remove some signal, and an optimum cut which gives the best statistical accuracy must be chosen.

The decay and scattering-angle cuts impose restrictions on the spectrometer angular acceptance and result in considerable data loss. Furthermore, they severely affect the (K,π) spectral shape, and require a refit of the bound-state peak region for each cut value. The effect of these cuts require a knowledge of the angular acceptance of the spectrometer.

Figure 10 is a plot of the density of events in the excitation energy-scattering angle plane. It gives a concise picture of the event distribution and shows the major background sources. One sees a dense vertical band of events at the extreme left. These are straight-through events, to be discarded by a scattering-angle cut. A diffuse broad band of events extends horizontally across θ, centered near an excitation energy, $EE = 20$ MeV. This region contains the quasifree or continuum events which represent the bulk of the (K,π) cross section (note that $EE = 0$ corresponds to 0 Λ binding energy). Two curved bands are apparent—the one near the center corresponds to $K^- \to \pi^0\pi^-$ decays, and the other, just at the lower right corner, corresponds to $K^- \to \mu\nu$ events. The bound-state region of interest is labelled "GS." The region of the GS cut is the region of useful (K,π) reactions in a search for the $M1$ spin-flip transition in $^{10}_{\Lambda}B$.

From these data, an evaluation was made of the true number of "bound-state" events for various decay cuts. The analysis efficiency varies from 0.84 to 0.14 for the range of decay cuts studied, with a fixed 40-mrad scattering-angle cut. The result of the weighted average over this range of decay cuts produces the following estimate for the number of bound-state events, corrected for spectrometer efficiency, N (bound-state events) $= 104\pm32$.

Three other corrections must be applied in the final estimate: a pion-decay correction for pions decaying between the target and exit dipoles (7.8%), a kaon-decay correction for decays occurring between the Cerenkov counter C_p and the target (3.0%), and a correction for target absorption of kaons and pions (6.4%). The result is, σ (bound state) $= 129\pm40$ μb/sr, at an effective mean reaction angle of 5.8°.

This estimate can be compared to the prediction of Ref. 10. From Ref. 10 there are three major contributors to the $\Delta L = 1$ transitions to the bound-state region. Correcting for the effective scattering angle, one finds σ (bound state) $= 95$ μb/sr, in reasonable agreement with experiment.

B. The $^7\mathrm{Li}(\pi,\pi')-^7\mathrm{Li}^*(478\ \mathrm{keV})$ test

The purpose of the test was to verify the operation of the germanium detector array under actual beam conditions. The lithium (π,π') reaction was chosen because of

its high cross section and because the first excited state is in an energy range expected for the hypernuclear γ rays.

The resulting spectra were readily accumulated, and the γ ray could be seen in the on-line, monitor spectra. Figure 11 shows a portion of the resulting spectrum after analysis. The total pion exposure for the 3.2 g/cm^2 target (92.5% ^{7}Li) was 2.045×10^9 pions (a running time of 18.3 h). The spectrometer was set at 15°.

The data were reduced with and without chamber tracking, which allowed us to evaluate the chamber tracking efficiency (80.2%) independently. As Fig. 11 shows, the 478-keV transition is significantly Doppler broadened. The amount of broadening is consistent with the component of momentum transfer perpendicular to the scattering plane for the (π,π') reaction at 800 MeV/c.

To calculate a cross section, it is necessary to evaluate several efficiency factors specific to the germanium detector array. These include intrinsic efficiency of the detector, and the geometric solid angle of the array. The product of these factors was found to be represented by the function,

$$\epsilon(E_\gamma)=\frac{0.040}{0.739+0.163(x/100)^{1.67}}\ (\mathrm{sr}/4\pi)\ , \qquad (6)$$

where x is the γ-ray energy in keV. The resulting efficiency, evaluated at 0.478 MeV, is 0.013 ± 0.002.

Because of electronic losses, there are additional efficiency factors to be considered. These arise from two factors: one is due to baseline recovery circuitry in the gated integrator, and the second is due to events which are sufficiently shifted by baseline noise to be indistinguishable from continuum background in the region of the peak. The first factor is measured by the ratio of events recorded in the ADC to the total $(K\pi\gamma)$ trigger events; the second is evaluated from the calibration pulser spectrum. These efficiencies were 0.682 and 0.784, respectively, resulting in a net γ-detection electronic efficiency of 0.534. Further corrections must be made for target absorption of the γ ray (12.2%) for data acquisition efficiency (83.3%), and for pion-decay loss (13.1%).

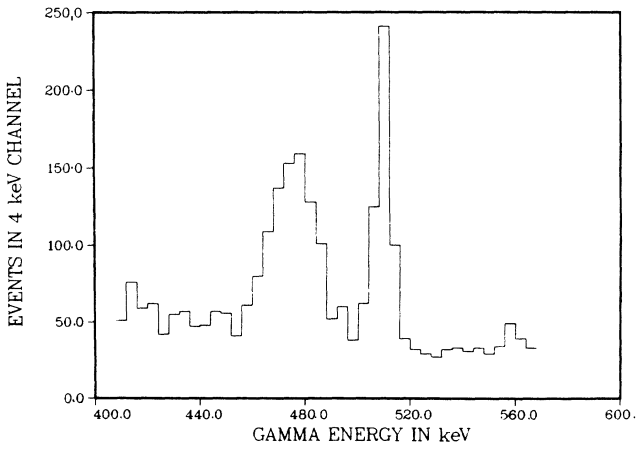

FIG. 11. A portion of the ^{7}Li$(\pi,\pi')^7$Li* (478-keV) spectrum.

One additional correction involves knowledge of the electron contamination of the pion beam. This is estimated at 24% based on estimates of Milner *et al.*[13] for LESB1.

A cross section value follows for the ^{7}Li$(\pi,\pi')^7$Li*(478-keV) reaction of 2.2 ± 0.3 mb/sr at 800 MeV and $\theta=15°$. We found no other reported measurements of this reaction for this range. However, Lee and Kurath[14] quote unpublished data for $p_\pi=270$ MeV/c which gives a measured cross section of ~2 mb/sr at 40° for a comparable momentum transfer, and they calculate a cross section of 0.85 mb at 0° at $E_\pi=162$ MeV.

V. RESULTS FROM THE THICK-SAMPLE ^{10}B$(K^-,\pi^-)^{10}_\Lambda$B EXPERIMENT

A. Observed spectrum

The major share of the running time was allocated to a search for the ground-state doublet transition from the ^{10}B$(K^-,\pi^-\gamma)^{10}_\Lambda$B reaction, using a thick, 12.28-gm/cm^2 ^{10}B sample. The sample was irradiated with a total of 1.716×10^{10} kaons at a nominal spectrometer setting of 3°. The beam line momentum was 800 MeV/c, and the central trajectory of the outgoing pion beam was 730 MeV/c.

The γ-ray spectrum in coincidence with the $^{10}_\Lambda$B bound-state region is shown in Figs. 12 and 13. This spectrum has been obtained by applying the appropriate time window cut as a function of γ-ray energy, as shown in Fig. 3. A portion of the spectrum is shown in the expanded scale of Fig. 13 where the region near 200 keV is shown in more detail. This is the region favored by Ref. 5 for the appearance of the ground-state doublet spin-flip transition. The expected event total is also shown in Fig. 12 as the solid curve.

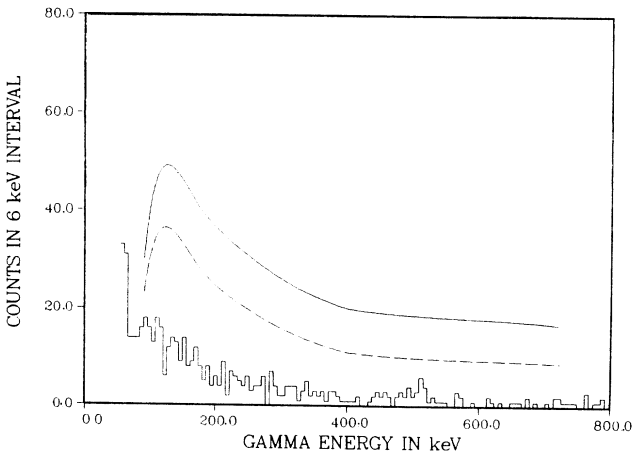

FIG. 12. The observed ^{10}B$(K^-,\pi^-\gamma)^{10}_\Lambda$B spectrum obtained with the optimum cuts described in the text. The solid line shows the expected event total predicted for the $^{10}_\Lambda$B ground-state doublet transition. The dashed line represents the 5% confidence limit for that transition, i.e., $P=0.05$ for the observation of peaks of less than the indicated strength.

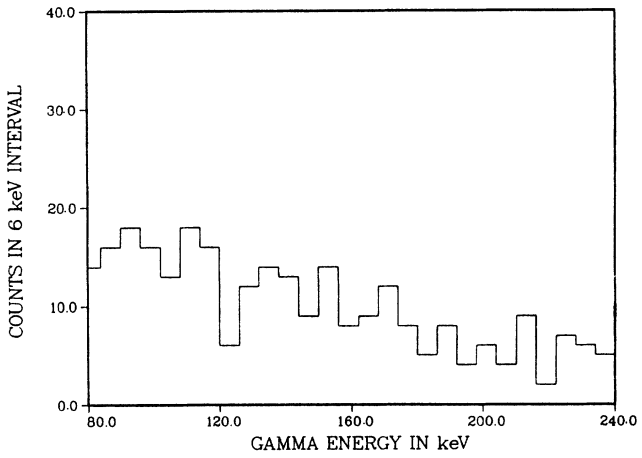

FIG. 13. An expanded portion of the spectrum of Fig. 15. The region shown is the expected location of the doublet transition predicted by Ref. 14.

Figures 12 and 13 show that there are *no observable* peaks which approach the predicted size in the bound-state excitation-energy region. The only significant peak occurs at the 511-keV annihilation radiation position, and this peak is attributed to Λ- and K-decay events.

B. Counting rate and sensitivity considerations

Because the use of a thick sample degrades the spectrometer resoltuion significantly, from ~ 3 to ~ 6 MeV (FWHM), the count-rate estimates were based on scaling the thin sample, where the bound state region can be more precisely identified, to the thick-sample data. The choice of a 3° nominal spectrometer setting gives an effective $\theta \simeq 5°$, over the spectrometer acceptance. The choice was made to give better discrimination against decays, which are concentrated at larger angles.

For each target the observed event rate in each portion of the γ-ray spectrum is expressed as

$$N_{\rm obs} = N_K (n\sigma) \Delta\Omega \, \text{eff(SYS)} \ , \tag{7}$$

and the ratios (thick/thin) are similarly expressed as,

$$R(N_{\rm obs}) = R(N_K) R(n\sigma) R(\Delta\Omega) R(\text{eff}) R(\text{abs}) \ , \tag{8}$$

where R(abs) represents the ratio of target kaon absorption.

Those ratios are trivially evaluated from the run parameters, except for the efficiency factors, which were evaluated in the manner described previously for the thin sample ^{10}B and ^{7}Li$(\pi,\pi'\gamma)$ tests. The expected bound-state (BS) production from the thin-to-thick extrapolation, including sample absorption losses, was $N(\text{BS}) = 8090 \pm 2400$ events for ^{10}B.

The predicted number of bound-state γ-ray events, N_γ can be written

$$N_\gamma = N_{\rm obs} \cdot \text{BR}(E_\gamma) \epsilon(\text{abs}) \epsilon(E_\gamma) \epsilon(\text{electronic}) \ . \tag{9}$$

The branching ratio for the population of the 2^- member of the $^{10}_{\Lambda}$B doublet is $\text{BR}(E_\gamma) = 0.52$ from Ref. 10 leading to a cross section of 50 μb/sr. [Note that the (K,π^-) reaction in ^{10}B (gs spin $= 3^+$) can only populate the 2^- member by a $\Delta L = 1$ transition; the spin-flip amplitude is negligible.] The ϵ(abs) parameter represents the affect of γ-ray absorption in the target, and varies for 0.835 at 100 keV to 0.925 at 900 keV. The $\epsilon(E_\gamma)$ factor is identical to that presented in the ^{7}Li$(\pi,\pi')^7$Li*(478) section. The ϵ(electronic) efficiency factors were evaluated for the thick-sample runs using the same methods described for the lithium test case. A value of $\epsilon(\text{electronic}) = 0.383$ was derived, significantly lower than the lithium test case, due to the more severe noise contributions. This efficiency is sensitive to instantaneous count rate effects which exhibited strong variations across the beam spill, and from spill to spill, and represents the largest source of systematic uncertainty in this experiment.

The results of this calculation are presented as the solid line in Fig. 12, as expected event rate as a function of γ-ray energy. Also shown on that figure is the dashed line representing the 5% confidence level for the predicted peak size; i.e., the probability for observing a peak of that size or less is 0.05. Weak decay competition has been included in these curves.

The plot shows that the expected count rates are considerably larger than those recorded, by a factor of at least 4, and the observed rates are everywhere considerably lower than the 5% confidence level. This negative result rules out the presence of a spin-flip γ ray of the expected size in the ground state doublet $^{10}_{\Lambda}$B, in the region above 80 keV. Above 500 keV, the expected $M-1$ lifetimes become comparable to ionic slowing down times, so that Doppler broadening somewhat degrades the effective resolution function. We estimate, for example, the peak width to approach 7 keV at the upper end of our energy range, from this effect.

One important comment is to point out that the achieved signal sensitivity is adequate for detection of the spin-flip γ ray in spite of the low count rate. The most important parameter in background elimination is detector timing. In fact, the timing is even more important than the detector full energy peak efficiency.

C. Other γ rays

Although a null result is reported for the excitation range $4 < B_\Lambda < 12$ MeV in $^{10}_{\Lambda}$B, there are significant peaks in other excitation regions. The continuum or "quasi-free" excitation energy region was scanned in 8-MeV increments. Two apparently statistically significant peaks appear in the region $-12 < B_\Lambda < -20$ MeV. These are shown in Fig. 14, plotted in 6-keV bin widths, and they occur with the following energies and cross sections

$$\left.\begin{array}{l}\sigma = 59 \pm 17 \ \mu\text{b/sr} \\ \text{FWHM} = 10.4 \pm 4.2 \ \text{keV}\end{array}\right\} \text{at } E_\gamma = 442.1 \pm 2.1 \tag{10}$$

and

$$\left.\begin{array}{l}\sigma = 49 \pm 18 \ \mu\text{b/sr} \\ \text{FWHM} = 13.8 \pm 6.5 \ \text{keV}\end{array}\right\} \text{at } E_\gamma = 481.7 \pm 3.1 \ . \tag{11}$$

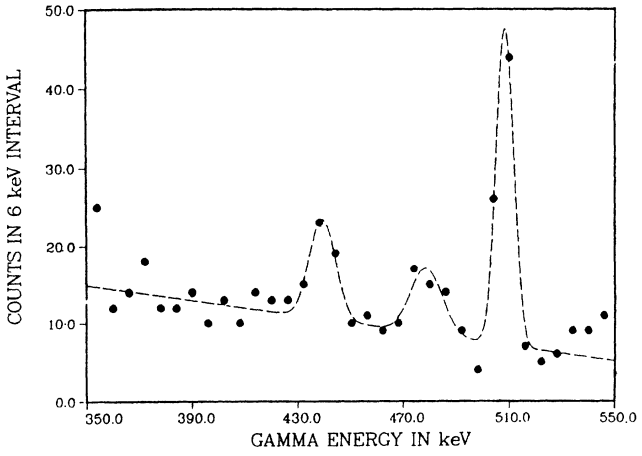

FIG. 14. A region of the $(K,\pi\gamma)$ gamma-ray spectrum near 500 keV for the region of $^{10}_{\Lambda}$B excitation between $B_\Lambda = -12$ and $B_\Lambda = -20$ MeV.

Both of these peaks are broader than the resolution function and the broadening is consistent with the Doppler shift expected at momentum transfers occurring for this excitation. Furthermore, the 481-keV γ ray appears both in the timed spectrum, and a spectrum obtained with the timing cut removed.

No definite identifications can be advanced for these lines. Figure 15 shows the reaction thresholds applicable in this experiment. Since the case (b) appears in both timed and untimed spectra, and since ^{7}Li*(478) can be produced in a variety of reactions (e.g., $K^- + {}^{10}\text{B} \rightarrow {}^{3}_{\Lambda}\text{He} + {}^{7}\text{Li}^*$) occurring in time, and $n + {}^{10}\text{B} \rightarrow {}^{4}\text{He} + {}^{7}\text{Li}^*(478)$ which occurs as an untimed background, it seems likely that peak (b) is attributable to ^{7}Li*.

Peak (a) is perhaps more interesting. First, we note that its energy, 442 keV, is close to that of the first excited states of the $A=7$, $J=\frac{3}{2},\frac{1}{2}$; $T=\frac{1}{2}$ isodoublet. It is in-

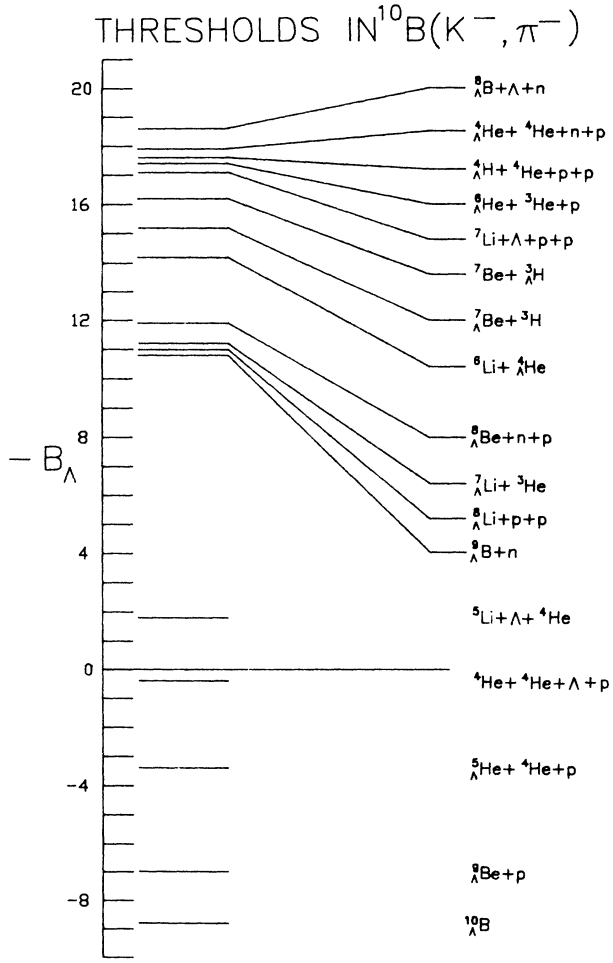

FIG. 15. The (K,π) thresholds for reactions on a ^{10}B target. The excitation is defined as 0 for $B_\Lambda = 0$, i.e., zero Λ binding in $^{10}_{\Lambda}$B.

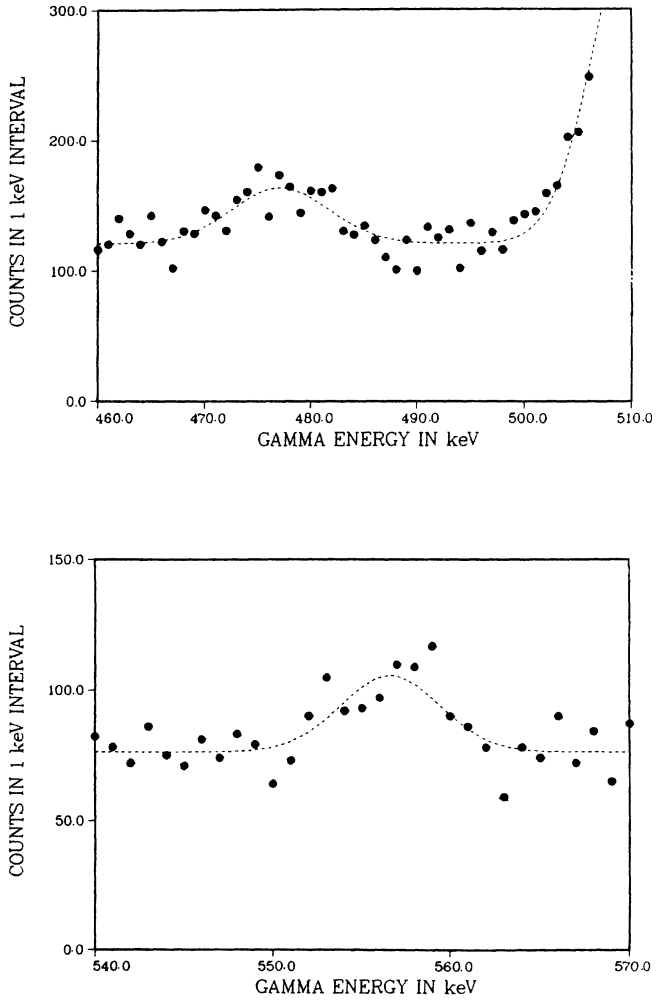

FIG. 16. A spectrum observed with all cuts relaxed. The regions shown are just below and just above the 511-keV annihilation peak.

tuitively attractive to associate this peak with a transition in the mass 7 core to which a Λ is coupled. We note further that the thresholds for either ${}^{8}_{\Lambda}$Li or ${}^{8}_{\Lambda}$Be production occur at this excitation, and further it is known from nuclear emulsion studies[15] with stopped kaons that ${}^{8}_{\Lambda}$Li is one of the most copiously produced hyperfragments.

There are two other peaks which are visible above background spectra where *all* cuts have been relaxed, including timing and spectrometer tracking cuts. One of these is again the 478 keV seen in the cut spectra; the other is a line near 558 keV. These transitions are shown in Fig. 16. The 478-keV peak appears Doppler broadened, while the 558 keV is consistent with our resolution function. The plausible interpretation for both of these peaks is slow neutron capture from the reactions $n+{}^{10}\mathrm{B}\rightarrow{}^{4}\mathrm{He}+{}^{7}\mathrm{Li}^{*}$ occurring in the boron target, and from $n+{}^{113}\mathrm{Cd}\rightarrow{}^{114}\mathrm{Cd}^{*}(558)$, which occurs in the Cd of the shields around the individual germanium detectors. The latter γ ray is the most intense after Cd neutron capture. A rough calculation shows that the event rate observed is consistent with the known neutron background from near the target region.

Several other lines were described as "candidate" lines in several preliminary reports of this experiment.[16–18] These lines, near 160 and 492 keV, did not survive subsequent analyses of the data, and they are attributable to fluctuations in the spectrum background. Both candidates can be rejected on the basis that they are far below the expected count rate calculated for a 50-μb/sr cross section in our experiment. Furthermore, the 160-keV fluctuation does not display the expected time distribution and is removed by suitable time cut.

VI. SUMMARY OF RESULTS AND DISCUSSION

A search has been made for a hypernuclear transition identified as the $M1$ spin-flip transition proceeding from the first excited 2^{-} state to the 1^{-} ground state of ${}^{10}_{\Lambda}$B. The search has been carried out with a sensitivity such that a transition with a strength of 25% (at 100 keV) of the expected line would be observed with a signal/noise ratio of unity. No such transition has been observed in the range 80 to 1 MeV. Below 80 keV, the transition would be virtually unobservable because of competition with weak decay.

These results are in rather sharp disagreement with the predictions of Ref. 5. In that paper, a set of two-body effective interactions is adopted, and predictions are made for the ${}^{10}_{\Lambda}$B and ${}^{8}_{\Lambda}$Li cases described above.

For ${}^{10}_{\Lambda}$B, the 2^{-} to 1^{-} transition energy is described as

$$\Delta E(2^{-}\rightarrow 1^{-})=0.62\Delta+1.36S_{\Lambda}+0.05S_{N}-1.49T \qquad (12)$$

The transition energy here is largely determined by the terms Δ, S, and T. If one assumes a consistent set of effective potential parameters for the p-shell hypernuclei, then the implication of our results is that the algebraic sum of the above terms is small—perhaps close to zero. Since the value of S_{Λ} has been constrained to be small by the Λ spin-orbit splitting observed in the hypernuclei ${}^{12}_{\Lambda}$C, ${}^{16}_{\Lambda}$O, and ${}^{13}_{\Lambda}$C, we conclude that the Δ parameter plays the major role in the splitting and the value adopted by Millener *et al.*[5] is likely too large.

On the other hand, as pointed out in Ref. 5, the difference in binding energies of ${}^{7}_{\Lambda}$Li and ${}^{7}_{\Lambda}$Be also strongly depend on the spin-spin parameter, Δ. Without refitting all other parameters, the choice of a Δ consistent with our results ($\Delta<0.22$) would result in a binding energy difference of $\Delta B=0.2$ MeV, or about half the experimental value. Thus there are now sufficient data to cast serious doubt on the accepted set of effective p-shell potential parameters.

The results of this search suggest that it may be difficult to observe directly the splitting of states formed by coupling the s_{Λ} to a p-shell nuclear core. This statement is also valid for the case of photoproduction of hypernuclei; where the sizable spin-flip amplitude permits the production of parity-unfavored states. It is rather doubtful whether magnetic spectrometers of sufficiently high resolution can be employed, in that case, to permit the separation of the closely-spaced doublets.

ACKNOWLEDGMENTS

The authors wish to acknowledge the valuable contributions of the Alternating Gradient Synchrotron (AGS) staff and the engineers and technicians of the Brookhaven National Laboratory (BNL) Medium Energy Group, E. Meier, A. Minn, B. Espensen, and Vito Manzella. Research was performed under Department of Energy and National Science Foundation support.

[a]Present address: University of New Mexico, Albuquerque, NM 87131.
[b]Present address: University of Illinois, Urbana, IL 61801.
[c]Present address: Mellon Institute, Pittsburgh, PA 15213.
[d]Present address: Princeton University, Princeton, NJ 08544.
[e]Present address: Los Alamos National Laboratory, Los Alamos, NM 87545.
[f]Present address: Wheaton College, Wheaton, IL 60187.
[g]Present address: Dynamics Technology Inc., Torrance, CA 90503.
[h]Present address: Brookhaven National Laboratory, Upton, NY 11973.
[i]Present address: University of Osaka, Osaka, Japan.
[j]Present address: Institute of Nuclear Studies, University of Tokyo, Tanashi, Tokyo 188, Japan.

[1]A. Bamberger, M. Faessler, U. Lynn, H. Piekarz, J. Piekarz, J. Pniewski, B. Povh, H. Ritter, and V. Soergel, Nucl. Phys. **B60**, 1 (1973).
[2]M. Bedjidian, A. Filipowski, J. Grossiord, A. Guichard, M. Gusakow, S. Majewski, H. Piekarz, J. Piekarz, and J. R. Pizzi, Phys. Lett. **62B**, 467 (1976); M. Bedjidian, E. Descroix, J. Grossiord, A. Guichard, M. Gusakow, M. Jacquin, M. Kudla, H. Piekarz, J. Pierkarz, J. Pizzi, and J. Pniewski, Phys. Lett. **83B**, 252 (1979).
[3]M. Bedjidian, E. Descroix, J. Y. Grossiord, A. Guichard, M. Gusakow, M. Jacquin, M. J. Kudla, H. Piekarz, J. Piekarz, J.

R. Pizzi, and J. Pniewski, Phys. Lett. **94B**, 480 (1980).
[4]M. May, S. Bart, S. Chen, R. Chrien, D. Maurizio, P. Pile, Y. Xu, R. Hackenburg, E. Hungerford, H. Piekarz, Y. Xue, M. Deutsch, J. Piekarz, P. Barnes, G. Franklin, R. Grace, C. Maher, R. Rieder, J. Szymanski, W. Wharton, R. L. Stearns, B. Bassaleck, and B. Budick, Phys. Rev. Lett. **51**, 2085 (1983).
[5]D. J. Millener, A. Gal, C. B. Dover, and R. H. Dalitz, Phys. Rev. C **31**, 499 (1985).
[6]A. Gal, J. M. Soper, and R. H. Dalitz, Ann. Phys. (N.Y.) **63**, 53 (1971).
[7]A. Gal, J. M. Soper, and R. H. Dalitz, Ann. Phys. (N.Y.) **72**, 445 (1972).
[8]A. Gal, M. M. Soper, and R. H. Dalitz, Ann. Phys. (N.Y.) **113**, 79 (1978).
[9]R. H. Dalitz and A. Gal, Ann. Phys. (N.Y.) **116**, 167 (1978).
[10]E. H. Auerbach, A. J. Baltz, C. B. Dover, A. Gal, S. H. Kahana, L. Ludeking, and D. J. Millener, Ann. Phys. (N.Y.) **148**, 381 (1983).
[11]P. H. Pile, in *Intersections Between Particle and Nuclear Physics (Steamboat Springs, Colorado, 1984)*, Proceedings of the Conference on the Interactions of Particles and Nuclear Physics AIP Conf. Proc. No. 123, edited by Richard E. Mischke (AIP, New York, 1984).
[12]R. M. Singru, K. B. Lal, S. J. Tao, and R. M. Lambrecht, At. Data Nucl. Data Tables **20**, 475 (1977).
[13]E. C. Milner, M. Barlett, G. W. Hoffman, S. Bart, R. E. Chrien, P. Pile, P. D. Barnes, G. B. Franklin, R. Grace, H. S. Plendl, J. F. Amann, T. S. Bhatia, T. Kozlowski, J. C. Peng, R. R. Silbar, H. A. Thiessen, C. Glasshauser, J. A. McGill, R. Hackenburg, E. V. Hungerford, and R. L. Stearns, Phys. Rev. Lett. **54**, 1237 (1985).
[14]T.-S. H. Lee and D. Kurath, Phys. Rev. C **21**, 293 (1980).
[15]M. Juric, G. Bohm, J. Klabuhn, U. Krecker, F. Wysotzki, G. Coremans-Bertrand, J. Sacton, G. Wilquet, T. Cantwell, F. Esmael, A. Montwill, D. H. Davis, D. Kielczewska, T. Pniewski, T. Tymieniecka, and J. Zakrzewski, Nucl. Phys. B **52**, 1 (1973).
[16]R. E. Chrien, in *Intersections Between Particle and Nuclear Physics* (Ref. 11), p. 841.
[17]M. May, in Proceedings of the International Symposium on Hypernuclear and Kaon Physics, Brookhaven National Laboratory, 1985, edited by R. E. Chrien [Nucl. Phys. **A450**, 179c (1985)].
[18]J. Derderien, Ph.D. thesis, Columbia University, 1987 (unpublished).